Diurnal variations of melt regions on the Greenland ice sheet

S. V. Nghiem[1], K. Steffen[2], R. Kwok[1], and W.-Y. Tsai[1]

[1]Jet Propulsion Laboratory, California Institute of Technology, Pasadena

[2]Cooperative Institute for Research in Environmental Sciences, University of Colorado, Boulder

Short title: DIURNAL VARIATIONS OF GREENLAND MELT REGIONS

Abstract. Melt regions on Greenland ice are mapped daily with the SeaWinds wideswath Ku-band scatterometer on the QuikSCAT satellite. The results reveal several pronounced warming and cooling events, and effects of topography are evident in the melt patterns. The resolution is sufficient to identify the Sukkertoppen Iskappe and its connection to the main ice sheet. Effects of zonal flow of Atlantic air are evident in the recurrence of the spatial distribution of melt regions in south Greenland. Determined by the sign of backscatter changes between morning and afternoon, positive and negative imbalance of the diurnal energy into the melting snow are observed over adjacent melt regions. An anomalous warming event, caused by turbulent mixing of warm air inversions, is detected in late September 1999 over the west flank of the southern Greenland, where the diurnal energy imbalance reversed over two consecutive days. Synoptic time-series images of melt regions are presented over the period from summer to the fall freeze-up. The satellite observations are verified well with in-situ measurements from Greenland Climate Network stations.

1. Introduction

The vast Greenland ice sheet plays an important role in regional and global climate [*Konzelmann and Ohmura,* 1995]. The massive Greenland ice sheet is an important component of the global hydrologic balance [*Ohmura,* 1996]. The energy absorbed by the snow pack can be doubled by small changes in snow-surface albedo [*Stroeve et al.,* 1997], which is significantly affected by surface snow melting [*Abdalati and Steffen,* 1995]. Because of the average slope of the ice sheet is less than 1°, small changes in air temperature result in large areal changes of dry and wet snow facies [*Abdalati and Steffen,* 1995]. The Greenland ice sheet is thus a sensitive indicator of the climate variability as demonstrated by the observed reduction in the melt area after the eruption of Mt. Pinatubo [*Abdalati and Steffen,* 1997].

Classification of Greenland snow melt regions have been investigated with different satellite data sets. With radiometer data from the Special Sensor Microwave Imager (SSM/I), Mote et al. [1993] used a single-channel threshold method, Steffen et al. [1993] applied the horizontally-polarized gradient ratio technique, and Abdalati and Steffen [1995] employed the cross-polarized gradient ratio approach. C-band synthetic aperture radar (SAR) data have been used to classify different snow facies, including dry and wet snow zones, on Greenland ice [*Partington,* 1998; *Fahnestock et al.,* 1993; *Jezek et al.,* 1993; *Drewry et al.,* 1991]. Absolute backscatter data from Ku-band scatterometers such as Seasat-A Satellite Scatterometer (SASS) and NASA Scatterometer (NSCAT) are also used to map Greenland melt areas with the imaging period of two weeks [*Long*

and Drinkwater, 1999].

In this paper, we delineate melt regions on the Greenland ice sheet using relative backscatter from daytime and nighttime satellite overpasses of the current SeaWinds scatterometer on the QuikSCAT satellite. Advantages of the melt mapping using new scatterometer data include: (a) high temporal coverage of the entire Greenland two times per day due to the very wide swath of the sensor, (b) high sensitivity of Ku-band backscatter to snow wetness with a dynamic range of more than one order of magnitude, (c) use of relative backscatter without depending on the absolute calibration, (d) determination of diurnal energy imbalance, and (e) verification of satellite results with in-situ data from Greenland Climate Network stations strategically located over different melt regions.

2. Satellite and Field Data

The QuikSCAT satellite was successfully launched at 7:15 p.m. Pacific Daylight Time on 19 June 1999 from the Vandenberg Air Force Base in California. The satellite carries the SeaWinds scatterometer for ocean wind measurements [*Graf et al.,* 1998]. The scatterometer has been collecting data at 13.4 GHz on both ocean and land. Backscatter data, at a radiometric resolution of 7 km $\times$ 25 km, are acquired with the vertical polarization (σ_{VV}) at a constant incidence angle of 54° over a conical-scanning swath of 1800 km, and with the horizontal polarization (σ_{HH}) at 46° over a 1400-km swath.

We select vertical-polarization data due to the very wide swath, which cover the

entire Greenland twice per day. The two local overpass times are around 6:20 and approximately 12 hours apart in a sun-synchronous orbit. The satellite orbit was stabilized, the scatterometer performance was verified, and the calibrated science data have been acquired since 19 July 1999 [*Tsai et al.,* 2000]. At that time, melt had occurred on the Greenland ice sheet, presenting the first opportunity to study diurnal variations of melt regions with the new data set.

In conjunction with the satellite data, we use hourly in-situ measurements including air temperature, net radiation, shortwave solar radiation, and wind speed. The field data are acquired at meteorological stations of the Program for Arctic Regional Climate Assessment (PARCA) Greenland Climate Network (GC-NET) [*Box et al.,* 1997]. Figure 1 shows the locations of GC-NET stations on the Greenland topographic map. In particular, stations Swiss Camp (69.569N, 49.311W) and Crawford Point 1 (69.882N, 46.974W), Dye-2 (66.481N, 46.280W), South Dome (63.149N, 44.817W), and KAR (69.700N, 33.000W) are strategically located in the west, central, south, and east regions, respectively, where snow melt typically occurs. Stations Saddle and NASA-SE would have provided additional data; however, both stations stopped transmitting via the satellite link since the spring of 1999, and the data will be available after the on-site visit in summer 2000.

3. Methodology

3.1. Backscatter Signature of Snow Melt

The principle of the melt region delineation is based on the high sensitivity of backscatter at Ku-band frequencies to moisture content or wetness in the snow cover. Ku-band backscatter of Greenland snow comes from subsurface volume scatterers located within different snow and ice structures. In fact, ground-based radar measurements of dry snow at Crawford Point indicate that the backscatter can be dominated by subsurface depth hoar and coarse-grain firn [*Jezek et al.,* 1994]. When the wetness in the snow surface layer increases, Ku-band wave energy is absorbed and subsurface scatterers are masked, resulting in a large decrease in backscatter.

The backscatter change is very sensitive to snow wetness [*Stiles and Ulaby,* 1980]. At 55° incidence angle, snow backscatter can drop more than 10 dB from the dry case to 3%-4% wetness cases [*Nghiem et al.,* 1999]. Figure 2 illustrates the sensitivity of snow backscatter to wetness. Ku-band backscatter is calculated from a physical snow scattering model [*Nghiem et al.,* 1995] for the vertical polarization at 56° incidence angle (SeaWinds scatterometer configuration). The calculated results also show more than 10 dB change from 0% to 3% volumetric snow wetness. For a given amount of change in wetness, the backscatter change is larger at the lower range of wetness values as seen in Figure 2.

To delineate melt regions on the Greenland ice sheet we exploit the relative difference in SeaWinds diurnal backscatter data. Because of the large swath, the entire

Greenland is measured in the early morning and again in the late afternoon. The energy for melting is provided by energy balance components including the conductive heat flux, the short and longwave radiation fluxes, and the turbulent sensible and latent heat fluxes [*Braithwaite et al.,* 1998]. These terms are determined by temperature, solar radiation, cloud cover, wind, and other meteorological conditions. Diurnal imbalances of these conditions lead to differences in the energy available for melting. Ablation, as an evaluation of melt energy, has a strong diurnal variation forced by diurnal changes in shortwave radiation and by nocturnal cooling due to outgoing longwave radiation and sublimation [*Braithwaite et al.,* 1998]. These variations result in the diurnal differences in snow wetness and consequently in backscatter differences at different diurnal overpasses of the SeaWinds scatterometer.

3.2. Approach

We subtract colocated data in the dB scale, equivalent to the ratio in the linear scale, between the day and night coverages over a resolution of 25 km. Given that the incidence angle of σ_{vv} is fixed at 54°, it is not required exact repeats of the orbit to obtain data consistently at the same incidence angle. Unlike NSCAT with variable incidence angles, the constant incidence angle of the SeaWinds scatterometer enables the use of the entire wideswath data, which make possible the diurnal coverages required in our approach.

For a backscatter change more than 1.8 dB, corresponding to the lower end of backscatter change in Figure 2, we classify the pixel to be in an active melt region.

While a transition between dry and wet conditions renders a large backscatter change as indicated in Figure 2, it is not necessary for the snow cover to switch from dry to wet condition for the melt region to be identified. The melt region can be delineated as long as there is a difference in wetness caused by the imbalance of energy into the ice between the daytime and the nighttime. For a positive backscatter change less than 1.8 dB and a negative change higher than -1.8 dB ($|\Delta\sigma_{VV}| < 1.8$), we classify the region with a green color which typically indicates the dry condition on the ice sheet.

An advantage of the method is that it is sensitive only to the region on the Greenland ice sheet with snow cover. Over bare land such as the barren coastal zone of Greenland, backscatter is not sensitive to diurnal changes and the method will classify the bare land with the green color. Thus, the method automatically eliminates bare land from the delineation of an active melt region on the Greenland ice sheet. Bare land has already a low albedo and thus the change in albedo of bare land is small compared to the snow covered region. Once the land becomes covered with snow undergoing an active melting process, the albedo change can be large and the method will detect the melt again.

Furthermore, when a snow-covered area becomes saturated with melt water during both daytime and nighttime, the diurnal backscatter change is weak and the area is classified with the green color. Again, the albedo change over such area is small. Another case is the exact overall balance of all geophysical conditions between day and night such that there is no change in snow wetness. However, this case is not likely to occur often over a large area, and this case means that there is no change in the diurnal

melt energy.

3.3. Diurnal Imbalance of Melt Energy

Not only a melt region can be delineated, Ku-band backscatter can also be used to determine the imbalance of the melt energy between morning and afternoon. Typically, the total energy flux into the ice in the early morning is low due to the nocturnal cooling during the previous night, corresponding to a lower snow wetness and higher backscatter. In a summer afternoon, the snow pack has absorbed energy from solar radiation during the day resulting in a higher snow wetness and a lower backscatter. However, this situation can occasionally be reversed and temperature in the early morning can be higher compared to the temperature in the following afternoon. Such a case can be related to a local weather event as observed with in-situ data from GC-NET.

We define the diurnal backscatter change as

$$\Delta\sigma_{VV} = \sigma_{VV}(local\ pm) - \sigma_{VV}(local\ am)$$

where all backscatter values are given in the dB scale. We assign a blue color over the melt region with negative values of $\Delta\sigma_{VV}$ as an indicator for the case of lower melt energy in the morning, and a red color for higher melt energy in the morning compared to that in the afternoon.

3.4. Spatial Pattern and Temporal Scale

Over a melt region delineated with either a blue or red color, we overlay contour lines for the backscatter change to indicate the intensity of the change. A larger

backscatter change corresponds to a lower range of snow wetness, and a smaller backscatter change is related to a higher value of snow wetness or a smaller change in the wetness. The contours are used to expose spatial patterns of snow wetness distribution over melt regions to study their relationship with geophysical characteristics over different regions of Greenland. Note that the approach does not depend on the absolute backscatter and, therefore, is independent of the absolute calibration and the long-term drift of the scatterometer gain, allowing the consistent interannual monitoring of melt regions. Finally, the high temporal resolution allow observations of weather events on the daily time scale.

4. Results

4.1. Summer Melt Patterns

We first study three cases at different times during the 1999 summer melt period. The results are presented in Figure 3 for both satellite observations and in-situ temperature measurements from four CG-NET stations including Dye-2 in the central, South Dome in the south, Crawford Point 1 in the west, and KAR in the east. The top three panels in Figure 3 show melt regions in late July (1999-07-21), the end of July (1999-07-31), and early August (1999-06-08).

Over the blue regions, 5 contour levels from 2 to 10 dB of backscatter change with 2-dB increments are plotted in white, yellow, light orange, dark orange, and red, respectively. Over the red regions, 5 contour levels for 2 to 10 dB backscatter change

are denote with dark blue, light blue, dark green, green, and light green. The locations of GN-NET stations are marked with the white '+' on the color maps. GC-NET temperature data are plotted in the lower panel and the three cases are indicated with the three vertical bands in the temperature plots, where the horizontal axis is marked with ticks at the beginning of the dates.

The results reveal both areal extents and spatial patterns of the melt regions. In the late July case (1999-07-21), an extensive melt band appears along the west side of Greenland and another smaller melt band along the northeast side. There is no significant melt observed at the locations of the four stations, except that Dye-2 is about the edge of the melt region. These observations agree well with the temperature data in the lower panel of Figure 3, showing air temperatures well below freezing, except Dye-2 temperature has come up to within just a degree below zero. The contour in the left map in the top of Figure 3 indicates a very small area with a strong backscatter change (8 dB) in the northern vicinity of Dye-2.

At the end of July (1999-07-31), the melt region is wide spread in much of the southern Greenland while the northeast melt band has shrunk to a small area as seen in the middle panel in the top of Figure 3. Both Crawford Point and Dye-2 are well within the blue melt region indicating that the melt energy in the morning was lower compared to that in the afternoon. In-situ temperatures at the two stations show a diurnal warming cycle from the cold condition in the morning to the warm condition above freezing in the afternoon. The field station data verify the results from SeaWinds which indicate: (a) melting occurs at the locations, and (b) there is more melt in the

afternoon. At South Dome, the contour show minimal wetness corresponding to the cold temperature there. The net radiation at Dye-2 peaked at 116 $W \cdot m^2$, an indication of overcast sky conditions, which was even higher than that on the previous day when the temperature had reached above zero. At KAR in the east, there is no melt observable by the satellite scatterometer in agreement with the low temperature measured by the station.

In the early August case (1999-08-06), the melt areas are still extensive in the southern Greenland; however, this melt region becomes fragmented compared to the case at the end of July. A large melt band in the northwest-southeast direction along the higher side passing Crawford Point; unfortunately the station data were not available. In contrast to the end-of-July case, Dye-2 station is located within the 'red' melt area, indicating a higher level of melt energy in the morning. This observation is verified with temperature data at Dye-2, showing higher melting temperatures in the morning as seen in the bottom panel of Figure 3. The contours in the right-hand map of Figure 3 suggests some melting in the surrounding of, but excluding South Dome station. Over the east side, the edge of the melt region extends up to the south of KAR station. In-situ temperatures at both stations were approaching $-1°C$ close to the melting condition as seen in Figure 3.

Maps of melt regions in Figure 3 reveal patterns related to the geophysical characteristics of Greenland. The west coastal region, along the western melt band on 1999-07-21, appears as green in the corresponding map because of the barren coastal land. The red contours in the middle map of Figure 3 show backscatter changes of

10 dB or larger in the surrounding of South Dome, passing Saddle, and extending to the north of Saddle. As discussed above, the backscatter change can be larger than 10 dB, and the larger change corresponds to the lower range of wetness value. In this respect, the melt pattern on 1999-07-31 indicates a lower wetness distribution over areas coincident with higher altitudes as seen in the topography presented in Figure 1. This pattern of the wetness distribution is well consistent with results by Stroeve and Steffen [1997] indicating that "the surface temperature of the Greenland ice sheet is strongly dominated by topography, with minimum surface temperatures associated with high elevation regions."

The relationship between the pattern of melt regions and the topography is even more obvious in the right-hand side map in Figure 3. The melt pattern exhibits four separated regions extended from Saddle station. The two melt regions in the north and south of Saddle are classified in blue with strong backscatter changes corresponding to morning low energy and low wetness over the higher elevations. The other two melt regions in the west and east of saddle appeared in red color with smaller backscatter changes for higher melt energy in the morning and higher wetness over the lower elevations. In this view, Saddle station appears to be strategically located at the center of a topographic saddle. Another feature that shows the close relation between the pattern of melt distribution and the topography is the green area similar to a boomerang shape in the southwest side below KAR station.

4.2. Seasonal Monitoring

We have derived daily maps of melt regions from the summer well into the fall season until early November 1999. The time-series includes more than 100 maps, from which we select representative results to present the seasonal variations of melt regions on the ice sheet in Figure 4. The time-series results show extensive melt in July and August from the west to the east of the southern Greenland with the largest melt areal extent in late July and early August. Later in August, the melt regions are more limited toward the west flank of the Greenland ice sheet. There occur minimal melt activities in September and later into the fall season. We compare the melt variations in Figure 4, derived from the satellite scatterometer, with in-situ temperatures measured at several GC-NET stations shown in the lower panel of Figure 3, especially for the times when the station data indicate warm conditions.

At Dye-2, temperatures (black curve in Figure 3) are above freezing and cooler in the morning of 24 July, close to freezing on 30 July, warmer in the morning on 3 August, close to freezing again on 7 August, and below freezing on the other dates. Dye-2 temperature records agree with the satellite time-series results showing Dye-2 station in the middle of the blue melt region on 24 July, at the melt edge on 30 July, at the south tip of the red melt region on 3 August, at the edge of the melt edge again on 7 August 1999. On the other dates, Dye-2 is either at the edge or in the dry region except on 15 August when Dye-2 is in the small red melt area. In this peculiar case, the temperature at Dye-2 is well below freezing indicating that the area should be dry. However, wind

speeds measured at Dye-2 show a strong three-fold increase from about 4 m/s to 12 m/s from morning to evening, which may correspond to a local weather event resulting in an energy balance more complicated than the indication by the air temperature alone.

At Crawford Point 1, the air temperature (blue curve in Figure 3) on 24 July has a strong increase from the cold condition in the morning to above freezing in the evening. At the time, the melt region extends from Dye-2 up to Crawford Point. For the other dates in July-August, Crawford temperatures are at or below freezing and the station is at the melt edge or in the dry region. An interesting case in the time-series results at KAR station is on 3 August when the temperature (orange curve in the lower panel of Figure 3) is high corresponding to the significant melt region in the east on the Greenland ice sheet. At South Dome, the temperature (red curve in Figure 3) just peak up a little above freezing on 30 July when the contours in the map indicate minimal melt at the station surrounded by strong backscatter changes. Otherwise, the image series shows mostly dry condition at South Dome.

The melt patterns in the time series also exhibit recurrences that are related to geophysical characteristics of the ice sheet. The arrows marked on the maps of 11, 15, and 19 of August point to a recurring feature connecting the internal melt region on the ice sheet and extending toward the shore line on the west coast. This feature coincides with the Sukkertoppen Iskappe and its connection to main ice sheet. This is a demonstration of the resolution of the QuikSCAT/SeaWinds data that is sufficient to pick up the melt features even on the smaller ice caps surrounding the ice sheet.

Comparing the melt patterns on 30 July and 7 August in Figure 4, we observe

the recurrence of melting at Dye-2, whereas the regions north and south show no melt signal. These north and south regions occurred at about the same locations in the images corresponding the two different dates. This pattern can be explained by the zonal flow of Atlantic air from east to west, commonly found in that region during summer. The region at Dye-2 is in direct line of the airflow over the saddle region, a depression between South Dome in the south and Summit in the north.

4.3. September Warming Event

In September, air temperatures are usually below freezing and no significant melt area is detected. However, the scatterometer clearly delineates an extensive melt band on 21 and 22 September 1999. This melt band is located along the west flank of the southern Greenland ice sheet as presented in Figure 5. Moreover, the melt region appeared in blue on 21 September indicates a higher melt energy with more wetness in the afternoon as seen in the left map in Figure 5. On the next day, the same melt region turned red suggesting a depletion of melt energy into the ice sheet with less wetness in the afternoon as observed in the right map in Figure 5. Thus, the diurnal energy imbalance between morning and afternoon reversed over the two consecutive days.

This melt band extends to the north over Swiss Camp station providing in-situ data to study this isolated melt event. The in-situ data for air temperature, wind speed, shortwave solar radiation, and net radiation are plotted in the lower panels of Figure 5. On 21 September, the air temperature rose in the afternoon due to low level clouds (solar radiation decreased) and due to a strong increase in wind speed. The wind

increase is responsible of mixing warm air from the inversion at the top of the planetary boundary layer to the surface. This phenomenon has been discussed recently by Steffen et al. [1999]. The net radiation plot in Figure 5 shows a net positive gain into the ice sheet during the mid-day time period of 21 September. The warming effect results in the surface melt in the afternoon.

On 22 September, low level clouds had moved out of the area and were replaced by thick medium level clouds (Altos type), which can be seen in the low solar radiation values. Wind activities dropped quickly to the calm condition with the minimum wind below 1 m/s just after the noon time. The temperature plot in Figure 5 shows a decreasing trend from the early morning into the late night. The net radiation is precipitously depleted to the minimum at about the same time of the wind minimum as evident in the corresponding plot in Figure 5. The satellite scatterometer image on 22 September shows still a wet surface in the morning and the freezing in the afternoon. Thus, the warming event as verified with the strong temperature increase is responsible for the melt in the afternoon of 21 September and in the morning of 22 September as seen in the SeaWinds images. This case demonstrate that the temporal resolution of the SeaWinds scatterometer is sufficient to capture the short time scale of weather events.

5. Conclusions

Diurnal variations of melt regions on the Greenland ice sheet are studied from the summer melt to the fall freeze-up in 1999. Melt regions are delineated daily with relative backscatter measured by the SeaWinds scatterometer on the QuikSCAT

satellite. The imbalance of diurnal melt energy between morning and afternoon are also identified by the sign of the backscatter change. Satellite melt mapping results are verified with in-situ measurements from several GC-NET stations. Time-series melt images reveal melt regions and their patterns during the summer season. The wetness distribution patterns are shown to correlate with the topography of the Greenland ice sheet. Melt features are identified over the Sukkertoppen Iskappe and its connection to the main ice sheet. The influence of zonal Atlantic air flow on the spatial distribution of melt regions is observed in south Greenland. An anomalous warming event caused by turbulent mixing of warm air inversion on the short time scale is also detected on 21-22 September 1999. While relative backscatter is consistent in the monitoring of melt regions, absolute backscatter subject to a stable calibration can also give further information on the ice sheet. Combining active scatterometer and passive radiometer such as SSM/I can provide complementary data set to study Greenland melt regions. Future field experiments are necessary to develop geophysical model functions to determine quantitative wetness distribution over the melt regions.

Acknowledgments. The research described in this paper was carried out by the Jet Propulsion Laboratory, California Institute of Technology, under a contract with the National Aeronautics and Space Administration. The research by the University of Colorado was supported by grants from the National Aeronautics and Space Administration Polar Program.

References

Abdalati, W., and K. Steffen, Passive microwave-derived snow melt regions on the Greenland ice sheet, *Geophys. Res. Lett.*, *22*(7), 787-790, 1995.

Abdalati, W., and K. Steffen, The apparent affects of the Mt. Pinatubo eruption on the Greenland ice sheet melt extent, *Geophys. Res. Lett.*, *24*(14), 1997.

Box, J. E., K. Steffen, and J. Weber, Greenland Climate Network (GC-NET) data reference, *Rep. Vers. 5.0*, 19 pp., Coop. Inst. Res. Environ. Sci., U. Colorado, Boulder, 1997.

Braithwaite, R. J., T. Konzelmann, C. Marty, and O. B. Olesen, Reconnaissance study of glacier energy balance in North Greenland, 1993-94, *J. Glac.*, *44*(147), 239-247, 1998.

Drewry, D. J., J. Turner, and W. G. Rees, The contribution of Seasat to ice sheet glaciology, *Int. J. Remote Sens.*, *12*(8), 1753-1774, 1991.

Fahnestock, M., R. Bindschadler, R. Kwok, and K. Jezek, Greenland ice sheet surface properties and ice dynamics from ERS-1 SAR imagery, *Science*, *32*(262), 1530-1534, 1993.

Graf, J. E., W.-Y. Tsai, and W. L. Jones, Overview of the QuikSCAT mission–A quick deployment of a high resolution, wide swath scanning scatterometer for ocean wind measurement, paper presented at *Southeastcon'98,* Orlando, FL, Apr. 1998.

Jezek, K. C., M. R. Drinkwater, J. P. Crawford, R. Bindschadler, and R. Kwok, Analysis of synthetic aperture radar data collected over the southwestern Greenland, *J. Glac.*, *39*(131), 119-132, 1993.

Jezek, K. C., P. Gogineni, and M. Shanableh, Radar measurements of melt zones on the Greenland ice sheet, *Geophys. Res. Lett.*, *21*(1), 33-36, 1994.

Konzelmann, T., and A. Ohmura, Radiative fluxes and their impact on the energy balance of

the Greenland ice sheet, *J. Glac.*, *41*(139), 490-502, 1995.

Long, D. G., and M. R. Drinkwater, Cryosphere applications of NSCAT data, *IEEE Trans. Geosci. Remote Sens.*, *37*(3), 1671-1984, 1999.

Mote., T. L., M. R. Anderson, K. C. Kuivinen, and C. M. Rowe, Passive microwave-derived spatial and temporal variations of summer melt on the Greenland ice sheet, *Ann. Glaciol.*, *17*, 233-238, 1993.

Nghiem, S. V., R. Kwok, S. H. Yueh, J. A. Kong, C. C. Hsu, M. A. Tassoudji, and R. T. Shin, Polarimetric scattering from layered media with multiple species of scatterers, *Radio Sci.*, *30*(4), 835-852, 1995.

Nghiem, S. V., M. Sturm, D. K. Perovich, B. Taras, B. Elder, and W.-Y. Tsai, Alaska snow experiment for applications of scatterometry to snow remote sensing, paper presented at American Geophysical Union Fall Meeting, San Francisco, California, Dec. 13-17, 1999.

Ohmura, A., M. Wild, and L. Bengtsson, A possible change in mass balance of Greenland and Antarctic ice sheets in the coming century, *J. Clim.*, *8*, 2124-2135, 1996.

Partington, K., Discrimination of glacier facies using multi-temporal SAR data, *J. Glac.*, *44*(146), 42-53, 1998.

Steffen, K., W. Abdalati, and J. Stroeve, Climate sensitivity studies of the Greenland ice sheet using satellite AVHRR, SMMR, SSM/I, and in situ data, *Meteorol. Atmos. Phys.*, *51*, 239-258, 1993.

Steffen, K., W. Abdalati, and I. Seherjal, Faceted crystal formation on NE-Greenland low accumulation region, *J. Glac.*, *45*(149), 63-68, 1999.

Stiles, W. H., and F. T. Ulaby, The active and passive microwave response to snow parameters.

1. Wetness, *J. Geophys. Res.*, *85*(C2), 1037-1044, 1980.

Stroeve, J., A. Nolin, and K. Steffen, Comparison of AVHRR-derived and in situ surface albedo over the Greenland ice sheet, *Remote Sens. Environ.*, *62*, 262-276, 1997.

Stroeve, J., and K. Steffen, Variability of AVHRR-derived clear-sky surface temperature over the Greenland ice sheet, *J. Applied Meteorol.*, *37*, 23-31, 1998.

Tsai, W.-Y, C. Winn, J. N. Huddleston, B. Stiles, M. Spencer, S. Dunbar, and S. V. Nghiem, SeaWinds on QuikSCAT: Overview of sensor system and post-launch calibration/verification (abstract), *Proc. Progress In Electromag. Res. Symp.*, Cambridge, Massachusetts, 2000.

R. Kwok, S. V. Nghiem, W.-Y. Tsai, Jet Propulsion Laboratory, California Institute of Technology, 4800 Oak Grove Drive, MS 300-235, Pasadena, CA 91109. (e-mail: Ronald.Kwok@jpl.nasa.gov; Son.V.Nghiem@jpl.nasa.gov; Wu-Yang.Tsai@jpl.nasa.gov)

K. Steffen, Cooperative Institute for Research in Environmental Sciences, University of Colorado, Campus Box 216, Boulder, CO 80309. (e-mail: Konrad.Steffen @colorado.edu)

Received _____

Figure 1. Locations of Greenland Climate Network stations on the topographic map

Figure 2. Ku-band backscatter σ_{VV} at 54° for different snow wetness

Figure 3. Images of melt regions on the Greenland ice sheet in July and August 1999 together with air temperatures measured at Dye-2 (black curve), Crawford Point 1 (blue curve), South Dome (red curve), and KAR (orange curve)

Figure 4. Time-series images of melt regions on the Greenland ice sheet

Figure 5. Images of melt regions corresponding to an anomalous warming event in September 1999

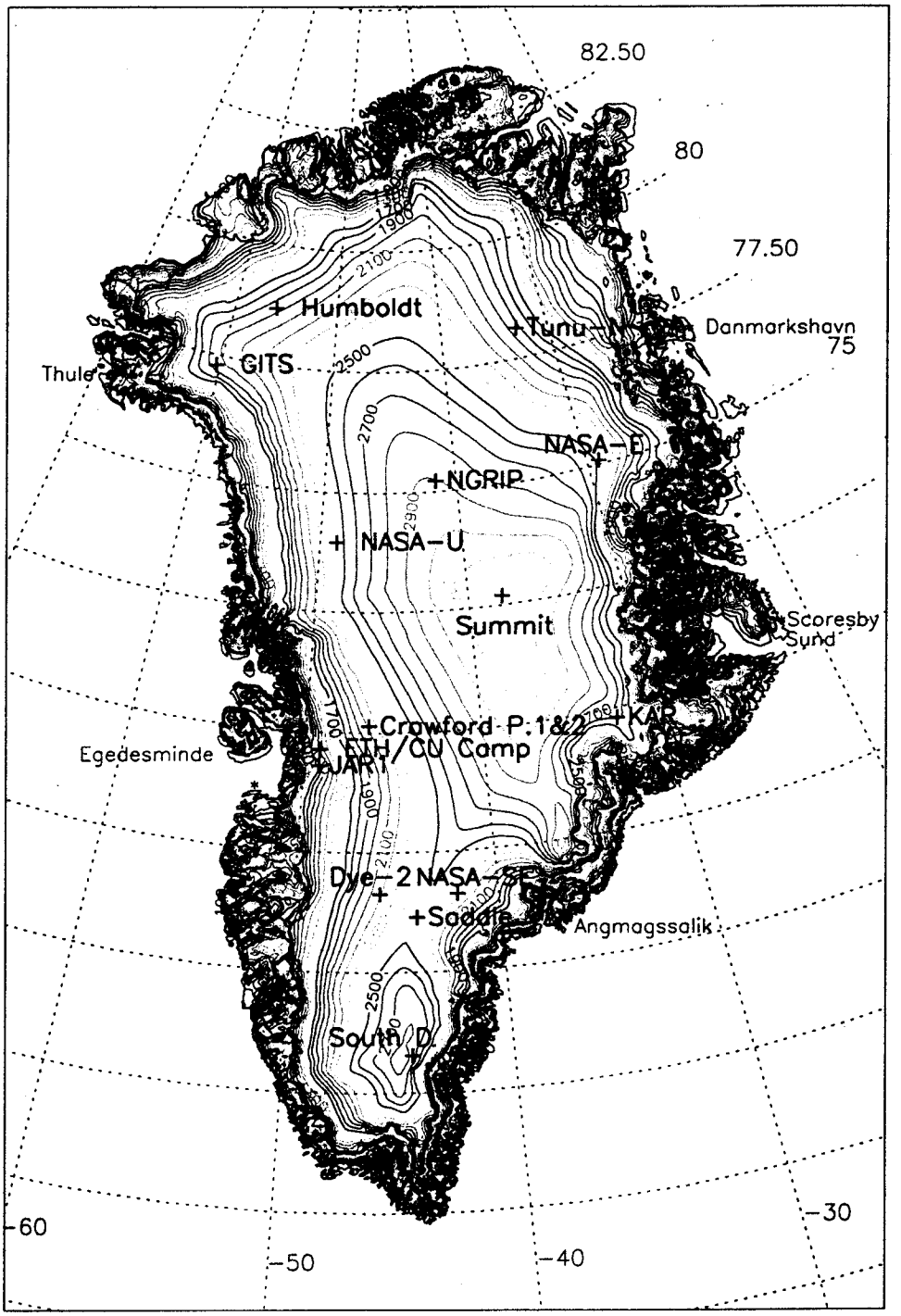
82.50
80
77.50
75
Humboldt
Tunu-N
Danmarkshavn
Thule
GITS
NASA-E
NGRIP
NASA-U
Summit
Scoresby Sund
Crawford P.1&2
KAR
Egedesminde
ETH/CU Camp
JAR1
Dye-2
NASA-S
Soddie
Angmagssalik
South Dome
1700
1900
2100
2300
2500
2700
2900
-60
-50
-40
-30

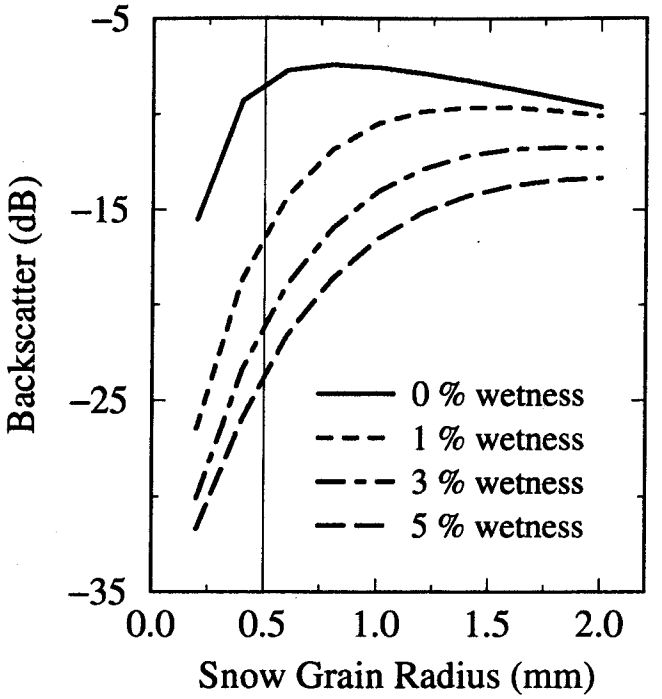

Figure 2 (Nghiem et al., 2000).

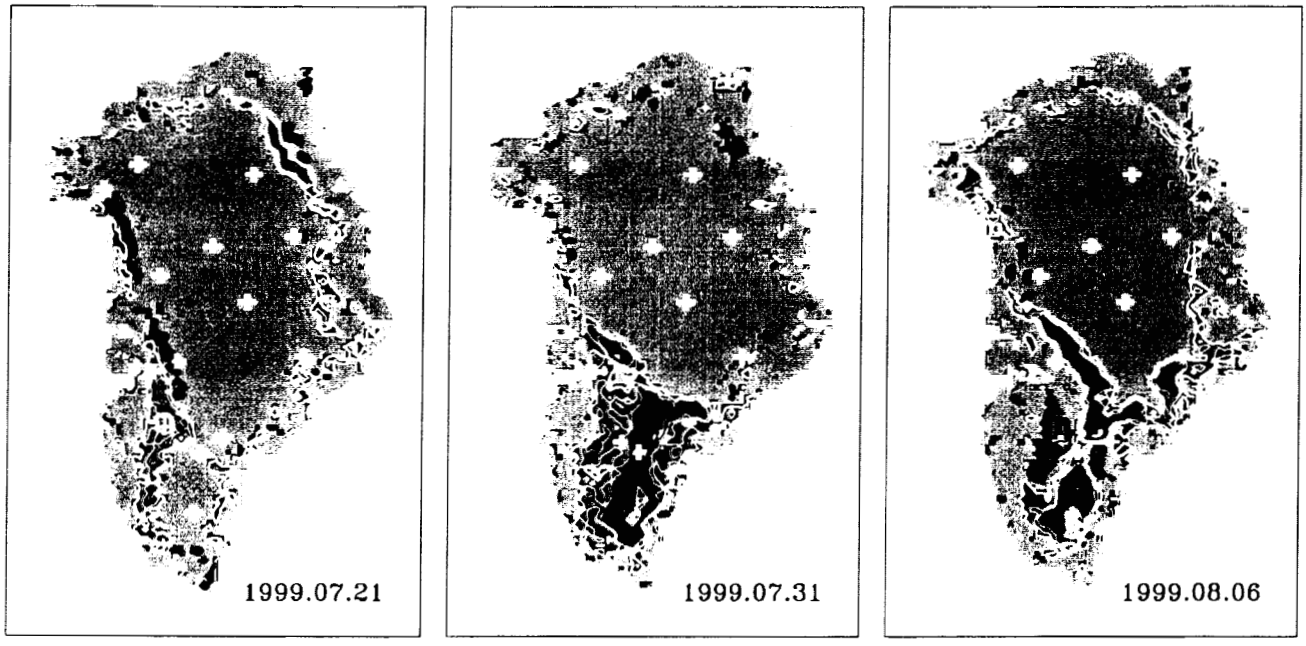

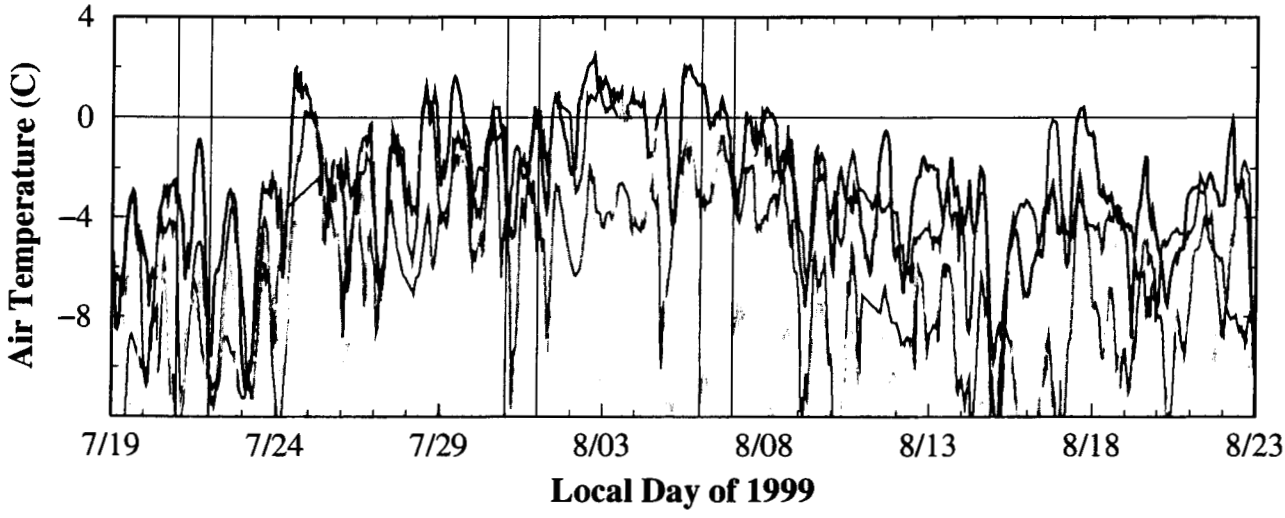

Figure 3 (Nghiem et al., 2000).

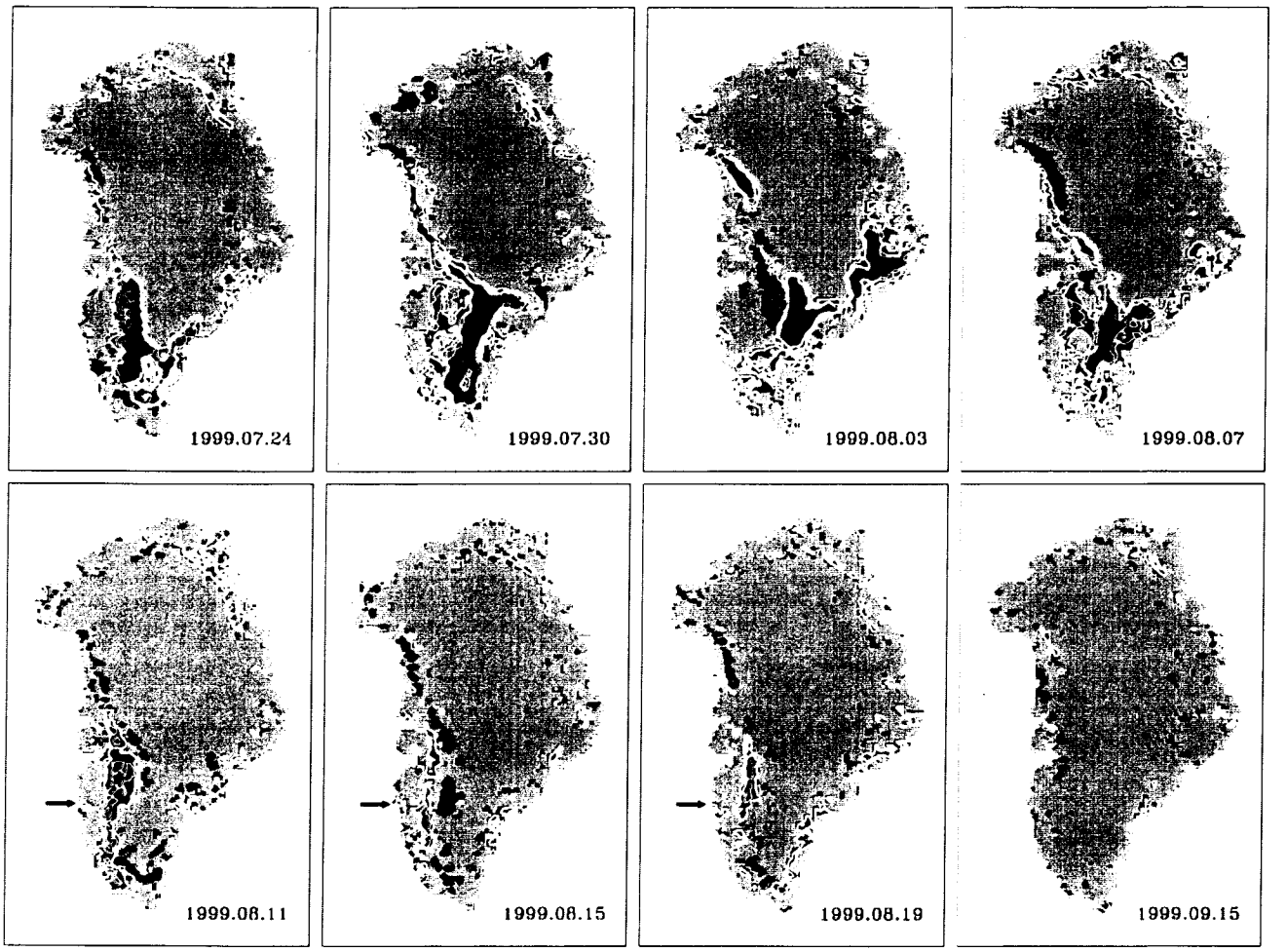

Figure 4 (Nghiem et al., 2000).

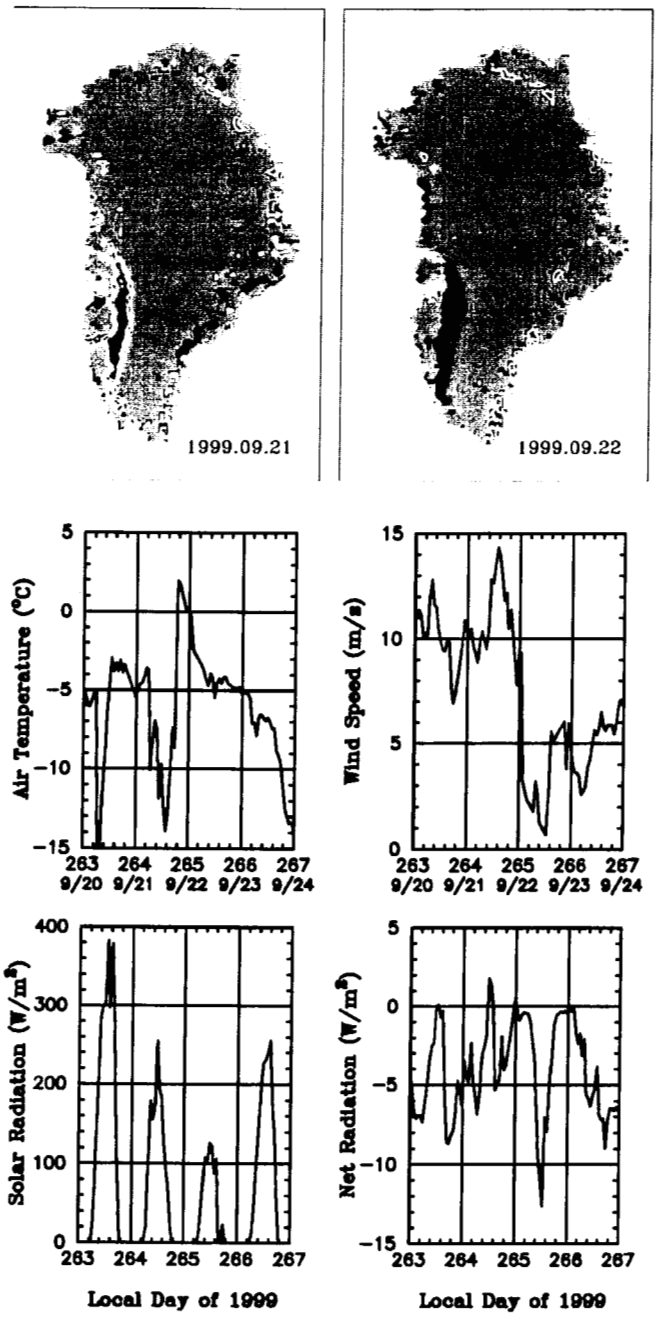

Figure 5 (Nghiem et al., 2000).